Learning Vector Representation of Content and Matrix Representation of Change: Towards a Representational Model of V1

Ruiqi Gao[1] RUIQIGAO@UCLA.EDU
Jianwen Xie[2] JIANWEN@UCLA.EDU
Song-Chun Zhu[1] SCZHU@STAT.UCLA.EDU
Ying Nian Wu[1] YWU@STAT.UCLA.EDU
[1]Department of Statistics, UCLA and [2]Hikvision Research Institute, USA

Abstract

This paper entertains the hypothesis that the primary purpose of the cells of the primary visual cortex (V1) is to perceive motions and predict changes of local image contents. Specifically, we propose a model that couples the vector representations of local image contents with the matrix representations of local pixel displacements caused by the relative motions between the agent and the surrounding objects and scene. When the image changes from one time frame to the next due to pixel displacements, the vector at each pixel is multiplied by a matrix that represents the displacement of this pixel. We show that by learning from pair of images that are deformed versions of each other, we can learn both vector and matrix representations. The units in the learned vector representations resemble V1 cells. The learned vector-matrix representations enable prediction of image frames over time, and more importantly, inference of the local pixel displacements caused by relative motions.

1. Introduction

David Hubel and Torsten Wiesel won the Nobel Prize for Physiology or Medicine in 1981 for their discovery of simple and complex cells in the primary visual cortex or V1 (Hubel & Wiesel, 1959). Figure 1(a) illustrates the V1 area. Hubel and Wiesel discovered that cells in V1 of the cat brain responded to bars of different locations, orientations and sizes, and each cell responded to a bar at a particular location, orientation and scale. See Figure 1(b). Some V1 cells are called simple cells,

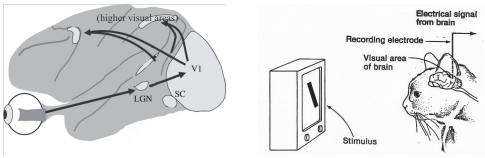

(a) (b)

Figure 1. (a) Primary visual cortex or V1 is the first step in representing retina image data. (b) Cells in V1 respond to bars of different locations, orientations and sizes. Sources: Internet.

which behave like linear wavelets. A mathematical model of a simple cell is Gabor wavelet (Daugman, 1985), which is sine or cosine plane wave multiplied by an elongate Gaussian function. The simple cells form pairs whose phases are $\pi/2$ apart, e.g., Gabor sine and cosine wavelets. A complex cell can be modeled by the sum of squares of the responses from a pair of simple cells. In (Sharma et al., 2000), the authors showed that V1 simple and complex cells can develop in the audio cortex if it receives input data from the retina. It would be interesting to understand the mathematical principle and model behind V1. This is the goal of this paper.

Since Hubel and Wiesel discovered the V1 cells using static stimuli while holding the head of the cat fixed, most of the existing methods learn V1-like units from static training images using sparse coding (Olshausen & Field, 1997) or independent component analysis (Bell & Sejnowski, 1997). There was also past work to learn complex cells from video sequences by assuming their responses vary slowly over time, i.e., the slowness constraint (Hyvärinen et al., 2003; Wiskott & Sejnowski, 2002). But let us step back and think about the purpose of vision. Only animals have vision, and only animals move in the 3D environment in order to catch preys or escape from the predators. When the animal moves,

the retina image keeps changing. The change of image is caused by the displacements of image pixels, and the displacements depend on the relative distances and motions between the animal and its surrounding objects.

This suggests that the main goal of vision, even at the lowest level or the earliest stage, is to perceive the environment under change, especially under relative motions, either due to self-motion of the agent or the motions of objects in the environment. In particular, the most basic representation in vision, such as the one in the primary visual cortex or V1, should intimately couple the representation of static image contents with the representation of the changes caused by the local displacements of pixels. In fact, the Gabor wavelets may be considered localized Fourier analysis which can represent spatial shifts by the changes of phases (Fleet & Jepson, 1990). Our work formalizes this idea, but our formalism only makes use of generic vector and matrix algebra, without making any assumptions about Fourier or Gabor basis functions. They emerge automatically in the learning process that minimizes simple loss functions.

Although computer vision has made tremendous progress in recent years, the focus has been on object recognition trained on big datasets of static images such as Imagenet (Deng et al., 2009; Krizhevsky et al., 2012). Indeed there have been research efforts on video data, yet the focus has been on high level tasks such as action recognition. The basic problem of finding a representational scheme that couples static image contents and pixel displacements has largely been overlooked. But this is the most basic problem that the visual system of, say, a bee or a rat, is intended to solve. In fact, recognizing thousands of object categories or generating captions of images is simply too much beyond what a basic visual system of a living organism is trying to accomplish. We believe the most basic function of vision is to separate appearance and geometry during self-motion or relative motion in order to navigate the 3D geometric environment.

To address this basic problem, this paper proposes a representational scheme that couples the vector representation of static image contents with the matrix representation of changes due to pixel displacements. See the following diagram (1) for an illustration, where the image is illustrated by the big rectangle. A pixel is illustrated by a dot. The local image content is illustrated by a small square around it. The displacement of the pixel is illustrated by a short arrow, which is within the small square. The vector representation of the local image content is represented by a long vector, which rotates as the image undergoes deformation due to the pixel displacements. See Section 3 for a detailed explanation of the mathematical notation in this diagram.

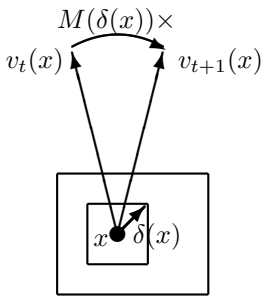

(1)

Our model consists of the following two parts:

(1) Vector representation of local image content. The local content around each pixel is represented by a high dimensional vector. Each unit in the vector is obtained by a linear filter. These local filters or wavelets are assumed to form a tight frame, i.e., the image can be reconstructed from the vectors using the linear filters as the basis functions. The justification for the tight frame assumption is that it ensures that the vector representation of the image has the isometry property, i.e., the inner product (or angle) between the vector representations of two images is the same as the inner product (or angle) between the two images themselves. This is particularly suitable when we model consecutive image frames over time, because the change of the vector reflects the change of the image.

(2) Matrix representation of local displacement. The change of the image from the current time frame to the next time frame is caused by the displacements of the pixels. Each possible displacement is represented by a matrix that acts on the vector. When the image changes according to the displacements, the vector at each pixel is multiplied by the matrix that represents the local displacement, in other words, the vector at each pixel is rotated by the matrix representation of the displacement of this pixel. Here we use the word "rotation" in a loose sense because we do not strictly enforce the matrix to be orthogonal to preserve the norm.

Two key features of our representational scheme are as follows.

(1) Separate representations of static image content and change due to motion. The change is effected by vector-matrix multiplication. Even though the transformation is linear, the matrix representation is a highly non-linear function of the displacement.

(2) Disentangled rotations. The vector at each pixel is

rotated by a corresponding matrix that represents the displacement. The transformation is not affected by the vectors of nearby pixels. That is, the rotations of the vectors at different pixels are disentangled. Thus the rotation of the vector at a particular pixel informs how this pixel moves, i.e., the perception of the motion at a pixel can be accomplished by detecting the rotation of the vector at this pixel, without the need to track the pixel over consecutive frames.

Furthermore, we divide the vector at each pixel into multiple sub-vectors, and assume that the rotations of the sub-vectors are also disentangled. That is, each sub-vector is rotated by a sub-matrix that depends on the pixel displacement, and the whole matrix is a block diagonal matrix with these sub-matrices being the diagonal blocks. Thus we only need to learn small sub-matrices.

We train our model on image pairs where in each pair, the second image is a deformed version of the first image, and the deformation is known. We estimate the encoding and decoding matrices for vector representation and the matrices that represent the given displacements by predictive loss. We consider two types of predictive losses. One is to predict the image of the next frame given the image of the current frame and the displacement field. The other is to predict the vectors of the next frame given the vectors of the current frame and the displacement field. Our experiments show that our method can learn V1-like filters. After learning the encoding matrices for vector representation and the matrix representation of the displacements, we can infer the displacement fields using the predictive losses.

The strength of the proposed model lies in its simplicity and naturalness. The static image contents and the motions of the pixels are encoded separately by vectors and matrices respectively, and they are coupled by matrix-vector multiplication. This representational scheme enables estimation of pixel displacement field, which, in turn, enables the perception of the 3D geometric environment, given the knowledge of self-motion.

2. Related work

Most well known models for the V1 representations are concerned with static images. The models assume that natural images are represented by linear superpositions of basis functions to be learned, while making various assumptions on the coefficients of the basis functions. The V1 units are identified with the basis functions and their activities are identified with the coefficients of the linear superpositions. Examples include sparse coding model (Olshausen & Field, 1997; Lewicki & Olshausen, 1999), independent component analysis (Hyvärinen et al., 2004; Bell & Sejnowski, 1997; van Hateren & Ruderman, 1998), and non-negative matrix factorization (Lee & Seung, 1999).

While the above models are based on top-down linear superpositions of basis functions, there are also models that are based on bottom-up linear filters. The V1 units are identified with the linear filters, and their activities are identified with the filter responses. Examples include the FRAME (Filters, Random field, And Maximum Entropy) model (Zhu et al., 1997), field of experts (Roth & Black, 2005), product of experts (Hinton, 2002), and sparse energy-based model (Teh et al., 2003).

A model that has both bottom-up filters and top-down basis functions is the restricted Boltzmann machine and its sparsified version (Hinton et al., 2006; Lee et al., 2009), and the model is similar to auto-encoder (Vincent et al., 2008). In our work, we adopt a tight frame representation, which is a linear auto-encoder.

More recently, the V1-like units have been learned by the deep convolutional neural networks for discriminative tasks (Krizhevsky et al., 2012; Zeiler & Fergus, 2014).

The V1 representation has also been learned on video data. For instance, the slowness criterion (Hyvärinen et al., 2003; Wiskott & Sejnowski, 2002) assumes that the features based on V1 responses vary slowly over time. The sparse coding model applied to the video data learns spatial-temporal basis functions (Olshausen, 2003). The independent component analysis has also been applied to video data (van Hateren & Ruderman, 1998). However, these models are not dynamic or predictive in that they do not predict the next time frame based on the current time frame.

The V1 representation has been learned by predictive task, see the recent paper (Singer et al., 2018) and the references therein. However, unlike our work, in (Singer et al., 2018) as well as related work, there are no explicit matrix representations of local pixel displacements, and the representations of local image contents are not explicitly coupled with the representations of local motions.

The predictive task in our work bears some similarity to the one in (Hinton et al., 2011), however, our representational scheme is very different. We do not learn to infer positions or poses.

In deep learning literature, it is a common practice to encode the signals as vectors or embed the signals into a vector space, so that linear interpolations and

arithmetics can be applied to the vectors, or the vectors preserve relationships between the signals in terms of their distances or inner products. However, it is much less common to encode the motions or actions by matrices that act on the vectors.

3. Representational model

Our model consists of vector representation and matrix representation. While vector representation corresponds to neuron activities, matrix representation corresponds to connection weights. There are two types of matrices. One type consists of the encoding and decoding matrices that map between the input image and the vector representation. The other type consists of the transformation matrices that represent the changes of the vector representation caused by the displacements of pixels. See diagram (1) in Section 1 for an illustration of the model.

3.1. Vector representation

Let $(\mathbf{I}(x), x \in D)$ be an image observed at a certain instant, where $x = (x_1, x_2) \in D$ is the 2D coordinates of pixel. D is the image domain (e.g., 128×128). We represent the image $\mathbf{I}$ by vectors $(v(x), x \in D_-)$, where each $v(x)$ is a vector defined at pixel x, and D_- may consist of a sub-sampled set of pixels in D (e.g., sub-sampled every 8 pixels). $V = (v(x), x \in D_-)$ forms a vector representation of the whole image.

We assume the vector encoding is linear and convolutional. Specifically, let $\mathbf{I}[x]$ be a squared patch (e.g., 16×16) of $\mathbf{I}$ centered at x. We can make $\mathbf{I}[x]$ into a vector (e.g., 256 dimensional). Let

$$v(x) = W\mathbf{I}[x],\ x \in D_-, \tag{2}$$

be the linear encoder, where W is the encoding matrix that encodes $\mathbf{I}[x]$ into a vector $v(x)$, and W is the same for all x, i.e., convolutional. The rows of W are the linear filters and can be displayed as a local image patch of the same size as the image patch $\mathbf{I}[x]$. We can write $V = \mathbf{WI}$, if we treat $\mathbf{I}$ as a vector, and the rows of $\mathbf{W}$ are the shifted or translated versions of W.

3.2. Tight frame and isometry

We assume that $\mathbf{W}$ is an auto-encoding tight frame, i.e., $\mathbf{I} = \mathbf{W}^\top V$, i.e.,

$$\mathbf{I} = \sum_{x \in D_-} W^\top v(x). \tag{3}$$

Thus, each row of W serves as a linear filter for bottom-up encoding, as well as a basis function for top-down decoding. Both the encoder and decoder can be implemented by convolutional linear neural networks.

The tight frame assumption can be justified by the fact that for two images $\mathbf{I}$ and $\mathbf{J}$, we have $\langle \mathbf{WI}, \mathbf{WJ} \rangle = \mathbf{I}^\top \mathbf{W}^\top \mathbf{WJ} = \langle \mathbf{I}, \mathbf{J} \rangle$, that is, the vector representation preserves the inner product, i.e., the representation has the isometry property. As a result, $\|\mathbf{WI}\| = \|\mathbf{I}\|$, $\|\mathbf{WJ}\| = \|\mathbf{J}\|$, thus the vector representation also preserves the angle.

Thus when the image $\mathbf{I}$ changes from $\mathbf{I}_t$ to $\mathbf{I}_{t+1}$, its vector representation V also changes from V_t to V_{t+1}, and the angle between $\mathbf{I}_t$ and $\mathbf{I}_{t+1}$ is the same as the angle between V_t and V_{t+1}.

3.3. Sub-vectors

The vector $v(x)$ can be high-dimensional. We further divide $v(x)$ into K sub-vectors, $v(x) = (v^{(k)}(x), k = 1, ..., K)$. Each sub-vector is obtained by an encoding sub-matrix $W^{(k)}$, i.e., $v^{(k)}(x) = W^{(k)}\mathbf{I}[x],\ k = 1, ..., K$, where $W^{(k)}$ consists of the rows of W that correspond to $v^{(k)}$. According to the tight frame assumption, we have $\mathbf{I} = \sum_{x \in D_-} \sum_{k=1}^{K} W^{(k)\top} v^{(k)}(x)$.

In our experiments, the rows of the learned $W^{(k)}$ tend to have similar orientations but different phases. This may be related to the modular organization or orientation columns in V1 (Hubel & Wiesel, 1959; Sharma et al., 2000).

3.4. Matrix representation

Let $\mathbf{I}_t$ be the image at time frame t. Suppose the pixels of $\mathbf{I}_t$ undergo local displacements, where the displacement at pixel x is $\delta(x)$. We assume that $\delta(x)$ is within a squared range Δ (e.g., $[-6, 6] \times [-6, 6]$ pixels) that is inside the range of $\mathbf{I}_t[x]$ (e.g., 16×16 pixels). Let $\mathbf{I}_{t+1}$ be the resulting image. Let $v_t(x)$ be the vector representation of $\mathbf{I}_t[x]$, and let $v_{t+1}(x)$ be the vector representation of $\mathbf{I}_{t+1}[x]$. Then $v_t(x) = (v_t^{(k)}(x), k = 1, ..., K)$, and $v_{t+1}(x) = (v_{t+1}^{(k)}(x), k = 1, ..., K)$.

The transition from $\mathbf{I}_t$ to $\mathbf{I}_{t+1}$ is illustrated by the following diagram, which shows how to predict $\mathbf{I}_{t+1}$ given $\mathbf{I}_t$ and the displacement field $(\delta(x), x \in D_-)$:

$$\begin{array}{ccc} v_t^{(k)}(x) & \xrightarrow{M^{(k)}(\delta(x))\times} & v_{t+1}^{(k)}(x) \\ W^{(k)} \uparrow & \uparrow & \downarrow W^{(k)\top} \\ \mathbf{I}_t & \xrightarrow{\delta(x)} & \mathbf{I}_{t+1} \end{array} \tag{4}$$

Specifically, we assume that

$$v_{t+1}^{(k)}(x) = M^{(k)}(\delta(x)) v_t^{(k)}(x), \tag{5}$$

for $x \in D_-, k = 1, ..., K$. That is, when $\mathbf{I}$ changes from $\mathbf{I}_t$ to $\mathbf{I}_{t+1}$, $v^{(k)}(x)$ undergoes a linear transformation, driven by a matrix $M^{(k)}(\delta(x))$, which depends on the local displacement $\delta(x)$. In terms of the whole vector $v(x) = (v^{(k)}(x), k = 1, ..., K)$, we have $v_{t+1}(x) = M(\delta(x))v_t(x)$, where $M(\delta(x)) = \text{diag}(M^{(k)}(\delta(x)), k = 1, ..., K)$ is the matrix representation of the local displacement $\delta(x)$.

We can animate the filters in $W^{(k)}$ using $M^{(k)}(\delta)W^{(k)}$ with different δ.

In addition to displacement, we can also use matrix to represent scaling or zooming, which can happen when the agent moves toward or away from an object.

3.5. Disentangled rotations

The linear transformations of the sub-vectors $v^{(k)}(x)$ can be considered as rotations. Here we use the word "rotation" in the loose sense without strictly enforcing $M^{(k)}(\delta)$ to be orthogonal. $v(x)$ is like a multi-arm clock, with each arm $v^{(k)}(x)$ rotated by $M^{(k)}(\delta(x))$. The rotations of $v^{(k)}(x)$ for different k and x are disentangled. Here disentanglement means algebraic disentanglement, not statistical disentanglement, i.e., given the matrix representations of local displacements, the rotation of a sub-vector does not depend on other sub-vectors.

The disentanglement between different positions x is the key feature of our model. Recall the change of image $\mathbf{I}$ is caused by the displacement of pixels, yet the rotations of sub-vectors $v^{(k)}(x)$ at different pixels x are disentangled. This enables the agent to sense the displacement of a pixel only by sensing the rotations of the sub-vectors at this pixel without linking pixels of consecutive frames.

3.6. Parametrization

The transition from $v_t^{(k)}(x)$ to $v_{t+1}^{(k)}(x)$ can be implemented by a linear recurrent neural network. However, the weight matrix $M^{(k)}(\delta(x))$ depends on the displacement, and the dependence can be highly non-linear.

We can discretize the displacement $\delta(x)$ into a finite set of possible values $\{\delta\}$, and we learn a separate $M^{(k)}(\delta)$ for each δ. We may use ℓ_2 regularization to encourage $M^{(k)}(\delta)$ to be a slowly varying function of δ, so that we can interpolate $M^{(k)}(\delta)$ continuously even if we only assume discrete δ.

We can also learn a parametric version of $M^{(k)}(\delta)$ as the second order Taylor expansion of a matrix-valued function of $\delta = (\delta_1, \delta_2)$, $M^{(k)}(\delta) = I + B_1^{(k)}\delta_1 + B_2^{(k)}\delta_2 + B_{11}^{(k)}\delta_1^2 + B_{22}^{(k)}\delta_2^2 + B_{12}^{(k)}\delta_1\delta_2$, where I is the identity matrix, and $B^{(k)} = (B_1^{(k)}, B_2^{(k)}, B_{11}^{(k)}, B_{22}^{(k)}, B_{12}^{(k)})$ are matrices of coefficients of the same dimensionality as $M^{(k)}(\delta)$.

3.7. Simple cells and complex cells

The units of $v^{(k)}(x)$ may be interpreted as the simple V1 cells, and the squared norm $\|v^{(k)}(x)\|^2$ may be interpreted as the complex V1 cells. When $v^{(k)}(x)$ rotates from $v_t^{(k)}(x)$ to $v_{t+1}^{(k)}(x)$, if we enforce $\|v_t^{(k)}(x)\|^2 = \|v_{t+1}^{(k)}(x)\|^2$, then $M^{(k)}(\delta(x))$ becomes an orthogonal rotation matrix. Then $\|v^{(k}(x)\|^2$ is invariant to the displacement and informs the identity of the object, while the rotation $M^{(k)}(\delta(x))$ is covariant with the displacement and changes the phase of $v^{(k)}(x)$. This disentangles appearance and motion.

3.8. Going beyond V1

The norm field $(\|v^{(k)}(x)\|, \forall k, x)$ and the inferred displacement field $(\delta(x), \forall x)$ can be fed into higher layers. The norm field can be used for object recognition, where the norms have geometrically explicit invariance property. The displacement field can be used for structure from motion, which may also feed back to V1 to refine the displacement field. We may also learn another layer of vector and matrix representations recursively at larger spatial and temporal scales to further compose the V1 units that move together. This can be a mathematical embodiment of Gestalt grouping.

4. Learning and inference

In this section, we describe the loss functions for learning the representation. The input data consists of the triplets $(\mathbf{I}_t, (\delta(x), x \in D_-), \mathbf{I}_{t+1})$, where $(\delta(x))$ is the given displacement field. The learned model consists of matrices $(W^{(k)}, M^{(k)}(\delta), k = 1, ..., K, \delta \in \Delta)$, where Δ is the range of δ. In the case of parametric $M^{(k)}$, we learn the B matrices in the second order Taylor expansion in subsection 3.6.

4.1. Loss functions for predictive learning

Given the training data, we can learn $W^{(k)}$ and $M^{(k)}(\delta)$ (or the B matrices that parametrize $M^{(k)}(\delta)$) by minimizing least squares predictive loss functions.

The key step of the prediction is disentangled vector rotation:

$$\hat{v}_{t+1}^{(k)}(x, \delta) = M^{(k)}(\delta)v_t^{(k)}(x) \quad (6)$$

$$= M^{(k)}(\delta)W^{(k)}\mathbf{I}[x]. \quad (7)$$

We can use the following predictive losses:

(1) Image-based predictive loss

$$L_1 = \left\| \mathbf{I}_{t+1} - \sum_{x \in D_-} \sum_{k=1}^{K} W^{(k)\top} \hat{v}_{t+1}^{(k)}(x, \delta(x)) \right\|^2. \quad (8)$$

This loss is based on the input images directly. It follows the diagram (4).

(2) Vector-based predictive loss

$$L_{2,x,k} = \left\| v_{t+1}^{(k)}(x) - \hat{v}_{t+1}^{(k)}(x, \delta(x)) \right\|^2. \quad (9)$$

This loss is based on the vectors computed from the input images.

In our learning algorithm, we learn the model either by the expectation of L_1 alone, or by a weighted sum of the expectations of L_1 and $\sum_{k=1}^{K} \sum_{x \in D_-} L_{2,x,k}$, where the expectations are taken over the training pairs of images and the corresponding displacement fields. The reason we want to incorporate $L_{2,x,k}$ is that we want to use it to infer the displacement field on testing pairs of images after learning the model. $L_{2,x,k}$ alone is not enough for learning because it does not explain the input image data. However, instead of pairing it with L_1, we can also pair $L_{2,x,k}$ with the tight frame auto-encoding losses on $\mathbf{I}_t$ and $\mathbf{I}_{t+1}$ to learn the model.

The loss function is invariant under orthogonal transformations of $v^{(k)}(x)$. Such gauge symmetry is friendly to gradient descent minimization.

In addition, we may add a term $L_{3,x,k} = (\|v_{t+1}^{(k)}(x)\| - \|v_t^{(k)}(x)\|)^2$ to enforce the stability of norm. Together with $L_{2,x,k}$, it forces $M^{(k)}(\delta)$ to be close to orthogonal.

4.2. Inference of motion

The learned representation can be used for predicting the next frame given the displacement field. This enables the agent to anticipate the sensory input during self-motion, because the displacement field can be predicted based on the 3D environment and self-motion. A more important application of the model is to infer the displacement field given a consecutive pair of image frames. After learning $(W^{(k)}, M^{(k)}(\delta), \forall k, \forall \delta)$, for a testing pair of $(\mathbf{I}_t, \mathbf{I}_{t+1})$, we can infer the pixel displacement field $(\delta(x), x \in D_-)$ by minimizing L_1 or $\sum_{k=1}^{K} L_{2,x,k}$ over $\delta(x)$.

The minimization of $\sum_{k=1}^{K} L_{2,x,k}$ is more convenient because it can be parallelized for different x. At each x, for all the possible candidate motions $\delta \in \Delta$, we can compute $\hat{v}_{t+1}^{(k)}(x, \delta) = M^{(k)}(\delta) v_t^{(k)}(x)$ for all δ in parallel. We then estimate $\delta(x)$ by comparing the predicted vectors $\hat{v}_{t+1}(x, \delta)$ with the observed vector $v_{t+1}(x)$, or more formally, by minimizing $\sum_{k=1}^{K} \|v_{t+1}^{(k)}(x) - \hat{v}_{t+1}^{(k)}(x, \delta)\|^2$ over all the candidate $\delta \in \Delta$. If we enforce norm stability, we only need to maximize the sum of alignments $A^{(k)}(x, \delta) = \left\langle v_{t+1}^{(k)}(x), \hat{v}_{t+1}^{(k)}(x, \delta) \right\rangle$ over δ. $A^{(k)}(x, \delta)$ may be interpreted as a cell that is sensitive to the velocity δ.

If we learn a parametric model for $M^{(k)}(\delta)$, we can also infer $(\delta(x))$ based on L_1 using gradient descent with an initialization of $(\delta(x))$ from random small values.

The inference step may enable us to learn the model in unsupervised manner without knowing $(\delta(x))$ in training, because we can use the inference algorithm as an inner loop in learning. We leave it to future investigation.

5. Experiments

We learn our model $(W^{(k)}, M^{(k)}(\delta), k = 1, ..., K)$ from image pairs $(\mathbf{I}_t, (\delta(x)), \mathbf{I}_{t+1})$. In our current implementation, the number of sub-vectors $K = 50$, and the number of units in each sub-vector $v^{(k)}(x)$ is 2. We also try other dimensionalities of sub-vector, e.g., 4 and 6. Each row of the encoding matrix $W^{(k)}$ is a filter. The size of the filter is 16×16, with a sub-sampling rate of 8 pixels in order to get D_-. We minimizes the loss functions in training using stochastic gradient descent implemented by the Adam optimizer (Kingma & Ba, 2014) ($lr = 0.003$) in TensorFlow.

5.1. Training data

The training data consist of $(\mathbf{I}_t, (\delta(x), \forall x \in D_-), \mathbf{I}_{t+1})$, where $(\delta(x), \forall x \in D_-)$ is the field of displacements. Such data can be obtained from existing optical flow datasets. We can also collect static images for $(\mathbf{I}_t)$ and simulate the displacement field $(\delta(x))$. The simulated displacement field is then used to deform $\mathbf{I}_t$ to obtain $\mathbf{I}_{t+1}$. In the following subsections, we first show the results learned from data with simulated displacement fields, and then display the results learned from real data.

Synthetic data. We choose an arbitrary category "rock" from MIT places205 dataset (Zhou et al., 2014), and randomly sample 1000 images for $\mathbf{I}_t$. The images are scaled to 128×128. Two types of displacement fields are generated and tested. (1) Global displacement field: a uniform displacement field, i.e., $\delta(x) = \delta, \forall x$. $\mathbf{I}_{t+1}$ is obtained by globally shifting $\mathbf{I}_t$ by δ. (2) Local displacement field: a displacement field with a mesh grid of control points. Specifically, we sub-sample the pixels of images into a $m \times m$ grid (e.g., 4×4 or 8×8), and randomly generate displacements on the

grid points, which serve as the control points for deformation. We use $m = 4$ in the experiments. Then $\delta(x)$ for $x \in D_-$ or $x \in D$ can be obtained by spline interpolation of the displacements on the control points. We get $\mathbf{I}_{t+1}$ by warping $\mathbf{I}_t$ using $\delta(x)$ for $x \in D$. Specifically, the pixel value of $\mathbf{I}_{t+1}$ is obtained by bilinear interpolation of the 4 nearest pixels around the corresponding pixel of $\mathbf{I}_t$ (Jaderberg et al., 2015).

When generating a displacement $\delta = (\delta_1, \delta_2)$, both δ_1 and δ_2 are randomly sampled from a range of pixels. For learning non-parametric version of $M(\delta)$, where the displacement $\delta(x)$ is discretized into a finite set of $\{\delta\}$, the range of displacement is set to $[-6, +6]$, with the step size of discretization equal to 1. For learning parametric version of $M(\delta)$, a smaller range of displacement is required in order to guarantee the accuracy of the second order Taylor expansion. The range is set to $[-3, +3]$. An advantage of using synthetic displacements is that at each mini-batch iteration, for each input image $\mathbf{I}_t$ in the batch, we can randomly generate $(\delta(x))$ online, which provides us training data with diverse displacement fields.

Real data. We learn from three real datasets: animal action dataset (Xie et al., 2018), MPI Sintel Flow (Butler et al., 2012) and FlyingChairs (Dosovitskiy et al., 2015). For videos, adjacent frames are taken as image pairs $(\mathbf{I}_t, \mathbf{I}_{t+1})$, which serves as the input to the model. For animal action dataset, we use the first 50 frames of the 30 videos for training. Images are scaled to 128×128. The ground truth $(\delta(x))$ are extracted by the FlowNet2 (Ilg et al., 2017), which is a state-of-art method to estimate the displacement field given a pair of images. For MPI Sintel Flow dataset, which contains 23 training videos and ground truth displacement fields, we choose the 18 videos of 50 frames, and use the first 40 frames for training. Images are scales to 192×192. For FlyingChairs dataset, which contains image pairs and the corresponding displacement field, we randomly choose 4000 pairs of images for training, with images scaled to 192×192.

5.2. Learned units

Figure 2 displays the learned units, i.e., rows of $W^{(k)}$, by minimizing the image-based predictive loss L_1 (Eqn. (8)). The units are learned with non-parametric $M(\delta)$, i.e., we learn a separate $M(\delta)$ for each displacement. Similar patterns can be obtained by using parametric version of $M(\delta)$. Please refer to the supplementary file for more results, including an animation of the movement of units with δ. V1-like patterns emerge on the learned units. Within each sub-vector, the orientations of learned units are similar, while the phases are different.

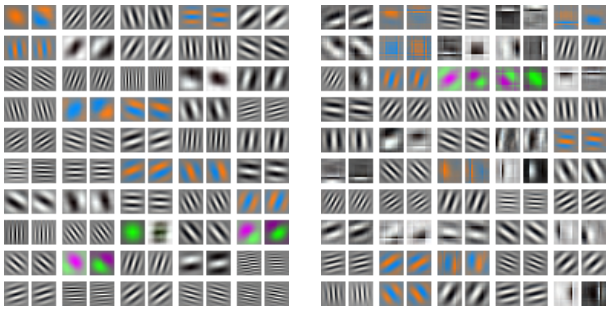

(a) Global displacement field (b) Local displacement field

Figure 2. Learned V1-like units with non-parametric $M(\delta)$. (a) Units learned using global displacement field; (b) Units learned using local displacement field. Each block shows two learned units within the same sub-vector.

Figure 3 displays the learned units with parametric $M(\delta)$. Similar to the ones learned with non-parametric $M(\delta)$, V1-like patterns emerge.

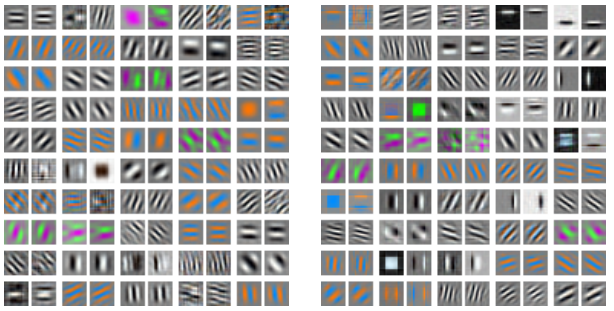

(a) Global displacement field (b) Local displacement field

Figure 3. Learned V1-like units with parametric $M(\delta)$. (a) Units learned using global displacement field; (b) Units learned using local displacement field. Each block shows two learned units within the same sub-vector.

5.3. Multi-step prediction

Given the starting frame $\mathbf{I}_0(x)$ and a sequence of displacement fields $\{\delta_1(x), ..., \delta_T(x), \forall x\}$, we can predict multiple steps of the subsequent frames $\{\mathbf{I}_1(x), ..., \mathbf{I}_T(x)\}$ using the learned model. We introduce a re-encoding process to improve the prediction. Specifically, at time t, after we get the next predicted frame $\mathbf{I}_{t+1}$, we take it as the observed frame at time $t + 1$, and re-encode it to obtain the latent vector v_{t+1} at time $t + 1$.

We randomly select 1000 testing images that are not observed during training from the same category of MIT places205, and for each testing image, randomly generate two types of displacement fields. Figure 10

displays several examples, learned with non-parametric version of $M(\delta)$. The predicted frames match the observed frames well. As a quantitative evaluation, we report the per pixel distance between the predicted frames and observed frames under different settings in table 1. For fair comparison, we restrict the range of displacement within $[-3, +3]$ for all the quantitative results.

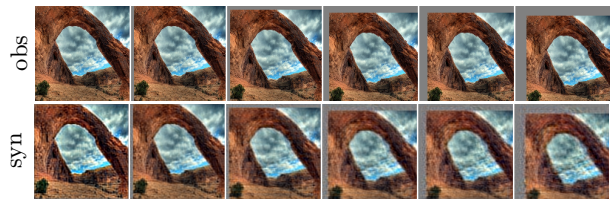

(a) Global shift to the bottom right

(b) Local deformation (e.g., seashore twisting)

(c) Local deformation (e.g., rock bending)

Figure 4. Examples of multi-step prediction. The top pair of sequences takes global displacement fields (global shift) as input, while the bottom two pairs of sequences take local displacement fields (local deformations) as input.

Table 1. Quantitative evaluations of multi-step prediction and inference of displacement field.

Displacement field	Parametrization of $M(\delta)$	Error of prediction	Error of inference
Global	No	9.659	0.455
	Yes	13.328	0.542
Local	No	7.623	0.552
	Yes	8.094	0.505

5.4. Inference of displacement field

We then test the learned representations in terms of inferring the displacement field ($\delta(x)$) between pairs of frames $(\mathbf{I}_t, \mathbf{I}_{t+1})$. $\mathbf{I}_t$ are the same 1000 unseen testing images as in 5.3, while $\mathbf{I}_{t+1}$ are obtained by warping $\mathbf{I}_t$ using generated displacement field. For learning with non-parametric $M(\delta)$, weighted sum of L_1 and $\sum_{k=1}^{K} L_{2,x,k}$ are used as the training loss, with the weight parameter equal to 1. After training, for each

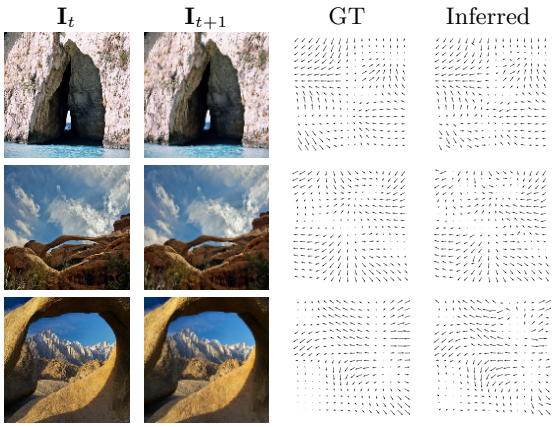

Figure 5. Examples of inference of displacement field. From left to right are $\mathbf{I}_t$, $\mathbf{I}_{t+1}$, ground truth displacement field and inferred displacement field respectively.

$x \in D_-$, we minimize $\sum_{k=1}^{K} L_{2,x,k}$ over all possible values of $\delta(x)$ to infer the displacement field. For learning with parametric $M(\delta)$, L_1 is used as training loss and $(\delta(x))$ is inferred by gradient descent on L_1 after training. Figure 5 displays some examples of the inferred displacement field, learned with parametric $M(\delta)$ and local displacement fields. We compute the average distance between the inferred and ground truth displacements under different settings, which is summarized in table 1.

5.5. Ablation study

We perform an ablation study to analyze the effect of several components of the proposed model. All the models in the ablation study are trained with parametric $M(\delta)$ and local displacement fields. The displacement inference is performed by gradient descent on L_1.

Dimensionality of sub-vectors. In the experiments, we assume that the number of units in each sub-vector $v^{(k)}(x)$ is 2, so that within each sub-vector, a pair of V1-like patterns are learned. However, we show that the dimensionality of sub-vectors does not have to be 2. Figure 6 shows the learned filters with the dimensionality equal to 4 or 6. Within each block, the orientations of learned patterns tend to be similar but the phases are different, which may be related to the orientation columns in V1 (Hubel & Wiesel, 1959; Sharma et al., 2000). For fair comparison, we fix the total number of units in the whole vector to 96, and change the number of units in each sub-vector. Table 2 summarizes the quantitative analysis of the models learned with different dimensionalities of sub-vectors, in terms of the performances of multi-step prediction and inference of displacement field. As the dimensionality of sub-vectors increases, the error rates of the two tasks

decrease first and then increase.

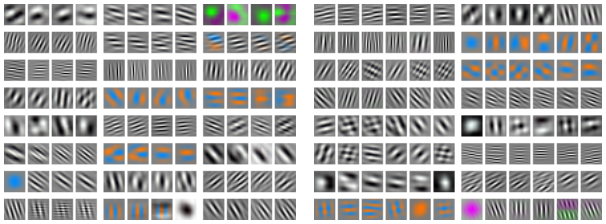

(a) Dimensionality = 4 (b) Dimensionality = 6

Figure 6. Learned V1-like units with different dimensionalities of sub-vectors.

Table 2. Quantitative analysis of the models learned with different dimensionalities of sub-vectors.

Sub-vector dim	2	4	6	8	12
Prediction error	8.684	8.387	7.486	7.926	8.412
Inference error	0.554	0.520	0.496	0.500	0.528

Table 3. Quantitative analysis of the models learned with different sub-sampling rates.

Sub-sampling rate	4	8	16
Prediction error	7.492	8.094	10.808
Inference error	0.658	0.505	0.565

Sub-sampling rate. Another factor that may affect the learned model is the sub-sampling rate in order to get $D_{\_}$. In the experiments, we use sub-sampling rate 8, which is half of the filter size. We can also increase or decrease the sub-sampling rate to make the adjacent image patches connected with each other more loosely or tightly. Table 3 summarizes the performance of learned models with different sub-sampling rates, in terms of multi-step prediction and inference of displacement field.

5.6. Learning from real data

We then try to learn the representational model from real data described in 5.1. The number of sub-vectors $K = 32$, with two units in each sub-vector. Figure 7 displays the learned units on three datasets: animal action, MPI Sintel Flow and FlyingChairs. The model is learned with non-parametric $M(\delta)$, and the displacement field is either from the ground truth displacements of the dataset or estimated by the FlowNet2 (Ilg et al., 2017). V1-like patterns emerge for all the models learned from the three datasets.

We test the multi-step prediction on MPI Sintel Flow and FlyingChairs datasets. Specifically, we randomly sample a starting frame from the unseen frames of videos, and use the sequence of subsequent displacement fields to predict the next several frames. Figure 8 shows some examples. Since FlyingChairs only contain image pairs and one-step ground truth displacement, one-step prediction is performed.

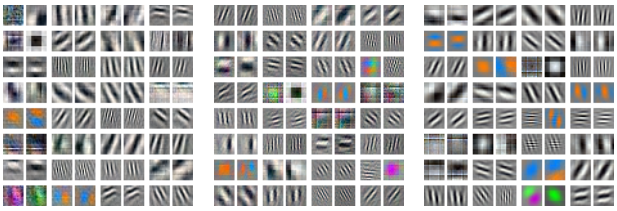

(a) Animal action (b) MPI Sintel Flow (c) FlyingChairs

Figure 7. Learned V1-like units on three real datasets.

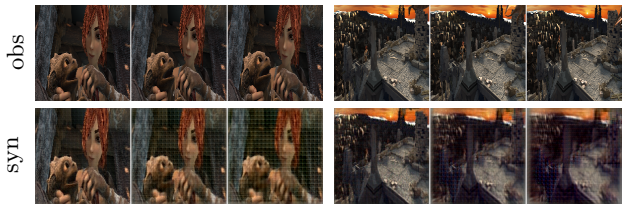

(a) Multi-step prediction on MPI Sintel Flow dataset

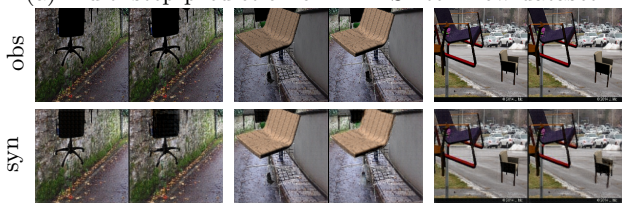

(b) One-step prediction on FlyingChairs dataset

Figure 8. Examples of frames prediction given the starting frame and subsequent displacement fields. (a) We show predicted frames at even time steps. The two examples are playing with animal and rotating of castle respectively. (b) Pairs of images with chairs flying are shown.

5.7. Scaling or zooming

We can extend the model to handle the scale change or zooming caused by the change of relative distance between the objects and the agent. Consider an image $\mathbf{I}_t$ of size $n \times n$. Let $x = (x_1, x_2)$ be a pixel. Let us assume that the center of the image is (0, 0). Suppose we zoom out the image to make it an image $\mathbf{I}_{t+1}$ of $m \times m$ by a factor $s = m/n$. Then each pixel x in $\mathbf{I}_t$ is moved to pixel sx in $\mathbf{I}_{t+1}$.

We can assume $v_{t+1}^{(k)}(sx) = \bar{M}^{(k)}(s)v_t^{(k)}(x)$. Here $\bar{M}^{(k)}(s)$ represent the change caused by scaling. The change from x to sx can be represented by pixel displacement. We can compose $M^{(k)}(\delta(x))$ and $\bar{M}^{(k)}(sx)$ at each pixel x, so that we can account for both shifting and scaling.

In the experiment, we assume $s = (n - \Delta x)/n$, where Δx is set to be within a range of pixels $[0, +6]$, with discretization step size equal to 1. We learn a model with non-parametric $M(\delta)$ and $\bar{M}(sx)$, using generated global displacement field. The learned units are show

in figure 9.

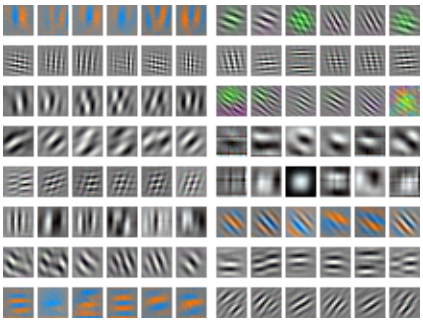

Figure 9. Learned V1-like units by learning from both shifting and scaling.

Figure 10 shows some multi-step prediction examples. The first 3 steps take a global shift δ as input, while the last 3 steps take a scaling factor s as input. By combining shifting and scaling, we are capable of predicting the 3D view change using the learned model.

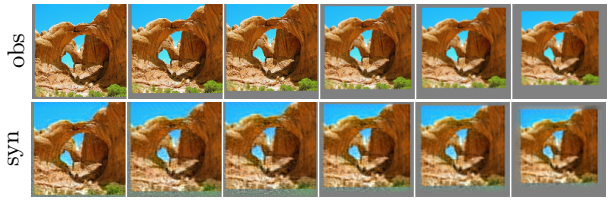

Figure 10. Example of multi-step prediction by combining shifting and zooming. The first 3 steps take a global shift δ as input, while the last 3 steps take a scaling factor s as input.

6. Conclusion

This paper proposes a representational model that couples the V1-like representations of static image contents with matrix representations of local pixel displacements caused by self-motion of the agent or the motions of the objects in the environment. The model encodes image contents and local motions separately and couples them by matrix-vector multiplication, which is applied in a pixel-wise disentangled manner. The model can be learned from unlabeled images undergoing global or local shifts. The learned model can be used to inferred the local motions in the testing images.

In our recent work (Gao et al., 2019), we have used vector and matrix representations to learn the grid cells for navigation, where we learn a vector representation of self-position coupled with a matrix representation of self-motion. The grid cells form an internal positioning system, whereas the V1 cells form a representation of external visual signals. In both systems, the motions are represented by matrices. The difference is that the self-motion in grid cells is a single 2D displacement vector, while the local motions in V1 form a displacement field. The self-motion and displacement field together enable inference of 3D representation of the environment.

In terms of general form of modeling, a recurrent network model is of the form $v_t = f(v_{t-1}, \delta_t)$, where v_t is the vector representation of the content, δ_t is the change, and f is a non-linear mapping. Our model is of the form $v_t = M(\delta_t)v_{t-1}$, where $M(\delta)$ is non-linear or perhaps non-parametric in δ, but the transition is linear in v_t, and may be interpreted as rotation. $M(\delta_t)$ is the matrix representation of the change δ_t.

The matrix representation of local displacements in our work is inspired by the group representation theory, where the group elements are represented by matrices acting on the vectors (Fulton & Harris, 2013). In our work, local displacements belong to 2D Euclidean group. The representation theory underlies much of modern mathematics and holds the key to the quantum theory (Zee, 2016). Perhaps it also underlies the visual and mortar cortex, where neurons form rotating sub-vectors driven by matrices representing groups of transformations. This may be called a rotationist-connectionist model, where the neuron activities encode sub-vectors, and the synaptic connections encode the matrices that rotate them.

Acknowledgment

The work reported in this paper is supported by DARPA XAI project N66001-17-2-4029; ARO project W911NF1810296; ONR MURI project N00014-16-1-2007; and a Hikvision gift to UCLA. We gratefully acknowledge the support of NVIDIA Corporation with the donation of the Titan Xp GPU used for this research.

References

Bell, A. J. and Sejnowski, T. J. The independent components of natural scenes are edge filters. *Vision research*, 37(23):3327–3338, 1997.

Butler, D. J., Wulff, J., Stanley, G. B., and Black, M. J. A naturalistic open source movie for optical flow evaluation. In A. Fitzgibbon et al. (Eds.) (ed.), *European Conf. on Computer Vision (ECCV)*, Part IV, LNCS 7577, pp. 611–625. Springer-Verlag, October 2012.

Daugman, J. G. Uncertainty relation for resolution in space, spatial frequency, and orientation optimized

by two-dimensional visual cortical filters. *JOSA A*, 2(7):1160–1169, 1985.

Deng, J., Dong, W., Socher, R., Li, L.-J., Li, K., and Fei-Fei, L. Imagenet: A large-scale hierarchical image database. In *Computer Vision and Pattern Recognition, 2009. CVPR 2009. IEEE Conference on*, pp. 248–255. IEEE, 2009.

Dosovitskiy, A., Fischer, P., Ilg, E., Häusser, P., Hazırbaş, C., Golkov, V., v.d. Smagt, P., Cremers, D., and Brox, T. Flownet: Learning optical flow with convolutional networks. In *IEEE International Conference on Computer Vision (ICCV)*, 2015. URL http://lmb.informatik.uni-freiburg.de/Publications/2015/DFIB15.

Fleet, D. J. and Jepson, A. D. Computation of component image velocity from local phase information. *International journal of computer vision*, 5(1):77–104, 1990.

Fulton, W. and Harris, J. *Representation theory: a first course*, volume 129. Springer Science & Business Media, 2013.

Gao, R., Xie, J., Zhu, S.-C., and Wu, Y. N. Learning grid cells as vector representation of self-position coupled with matrix representation of self-motion. *ICLR*, 2019.

Hinton, G. E. Training products of experts by minimizing contrastive divergence. *Neural Computation*, 14(8):1771–1800, 2002.

Hinton, G. E., Osindero, S., and Teh, Y.-W. A fast learning algorithm for deep belief nets. *Neural Computation*, 18:1527–1554, 2006.

Hinton, G. E., Krizhevsky, A., and Wang, S. D. Transforming auto-encoders. In *International Conference on Artificial Neural Networks*, pp. 44–51. Springer, 2011.

Hubel, D. H. and Wiesel, T. N. Receptive fields of single neurones in the cat's striate cortex. *The Journal of physiology*, 148(3):574–591, 1959.

Hyvärinen, A., Hurri, J., and Väyrynen, J. Bubbles: a unifying framework for low-level statistical properties of natural image sequences. *JOSA A*, 20(7):1237–1252, 2003.

Hyvärinen, A., Karhunen, J., and Oja, E. *Independent component analysis*, volume 46. John Wiley & Sons, 2004.

Ilg, E., Mayer, N., Saikia, T., Keuper, M., Dosovitskiy, A., and Brox, T. Flownet 2.0: Evolution of optical flow estimation with deep networks. In *IEEE Conference on Computer Vision and Pattern Recognition (CVPR)*, Jul 2017. URL http://lmb.informatik.uni-freiburg.de//Publications/2017/IMKDB17.

Jaderberg, M., Simonyan, K., Zisserman, A., et al. Spatial transformer networks. In *Advances in neural information processing systems*, pp. 2017–2025, 2015.

Kingma, D. P. and Ba, J. Adam: A method for stochastic optimization. *arXiv preprint arXiv:1412.6980*, 2014.

Krizhevsky, A., Sutskever, I., and Hinton, G. E. Imagenet classification with deep convolutional neural networks. In *NIPS*, pp. 1097–1105, 2012.

Lee, D. D. and Seung, H. S. Learning the parts of objects by non-negative matrix factorization. *Nature*, 401(6755):788, 1999.

Lee, H., Grosse, R., Ranganath, R., and Ng, A. Y. Convolutional deep belief networks for scalable unsupervised learning of hierarchical representations. In *International Conference on Machine Learning*, pp. 609–616, 2009.

Lewicki, M. S. and Olshausen, B. A. Probabilistic framework for the adaptation and comparison of image codes. *JOSA A*, 16(7):1587–1601, 1999.

Olshausen, B. A. Learning sparse, overcomplete representations of time-varying natural images. In *Image Processing, 2003. ICIP 2003. Proceedings. 2003 International Conference on*, volume 1, pp. I–41. IEEE, 2003.

Olshausen, B. A. and Field, D. J. Sparse coding with an overcomplete basis set: A strategy employed by v1? *Vision Research*, 37(23):3311–3325, 1997.

Roth, S. and Black, M. J. Fields of experts: A framework for learning image priors. In *CVPR*, volume 2, pp. 860–867. IEEE, 2005.

Sharma, J., Angelucci, A., and Sur, M. Induction of visual orientation modules in auditory cortex. *Nature*, 404(6780):841, 2000.

Singer, Y., Teramoto, Y., Willmore, B. D., Schnupp, J. W., King, A. J., and Harper, N. S. Sensory cortex is optimized for prediction of future input. *eLife*, 7: e31557, 2018.

Teh, Y. W., Welling, M., Osindero, S., and Hinton, G. E. Energy-based models for sparse overcomplete

representations. *Journal of Machine Learning Research*, 4(Dec):1235–1260, 2003.

van Hateren, J. H. and Ruderman, D. L. Independent component analysis of natural image sequences yields spatio-temporal filters similar to simple cells in primary visual cortex. *Proceedings of the Royal Society of London B: Biological Sciences*, 265(1412): 2315–2320, 1998.

Vincent, P., Larochelle, H., Bengio, Y., and Manzagol, P.-A. Extracting and composing robust features with denoising autoencoders. In *Proceedings of the 25th international conference on Machine learning*, pp. 1096–1103. ACM, 2008.

Wiskott, L. and Sejnowski, T. J. Slow feature analysis: Unsupervised learning of invariances. *Neural computation*, 14(4):715–770, 2002.

Xie, J., Gao, R., Zheng, Z., Zhu, S.-C., and Wu, Y. N. Learning dynamic generator model by alternating back-propagation through time. *arXiv preprint arXiv:1812.10587*, 2018.

Zee, A. *Group theory in a nutshell for physicists*. Princeton University Press, 2016.

Zeiler, M. D. and Fergus, R. Visualizing and understanding convolutional neural networks. In *ECCV*, 2014.

Zhou, B., Lapedriza, A., Xiao, J., Torralba, A., and Oliva, A. Learning deep features for scene recognition using places database. In *Advances in neural information processing systems*, pp. 487–495, 2014.

Zhu, S.-C., Wu, Y. N., and Mumford, D. Minimax entropy principle and its application to texture modeling. *Neural Computation*, 9(8):1627–1660, 1997.